

Hilbert space fragmentation imposed real spectrum of non-Hermitian systems

Somsubhra Ghosh¹, K. Sengupta¹ and Indranil Paul²

¹*School of Physical Sciences, Indian Association for the Cultivation of Science, Kolkata 700032, India*

²*Université Paris Cité, CNRS, Laboratoire Matériaux et Phénomènes Quantiques, 75205 Paris, France*

 (Received 20 July 2023; revised 26 December 2023; accepted 3 January 2024; published 24 January 2024)

We show that constraints imposed by strong Hilbert space fragmentation (HSF) along with the presence of certain global symmetries can ensure the reality of eigenspectra of non-Hermitian quantum systems; such a reality cannot be guaranteed by global symmetries alone. We demonstrate this insight for two interacting finite chains, namely the fermionic Nelson-Hatano and the Su-Schrieffer-Heeger models, none of which has a \mathcal{PT} symmetry. We show analytically that strong HSF and real spectrum are both consequences of the same dynamical constraints in the limit of large interaction, provided the systems have sufficient global symmetries. We also show that a local equal-time correlation function can detect the many-body exceptional point at a finite critical interaction strength above which the eigenspectrum is real.

DOI: [10.1103/PhysRevB.109.045145](https://doi.org/10.1103/PhysRevB.109.045145)

I. INTRODUCTION

Non-Hermitian many-body Hamiltonians are of great current interest for their relevance to open quantum systems and also for their novel properties without Hermitian analog [1–20]. These features include novel topological properties including the presence of so called exceptional points. At these points, certain energy eigenvalues are degenerate and the corresponding eigenfunctions coalesce. Across such points, these eigenvalues can transform from being real to complex [21–27]. Moreover, the nonequilibrium dynamics of such systems are of interest since they possess qualitatively different characteristics compared to that of their closed Hermitian counterparts [15–20]. Some such characteristics include the presence of athermal steady states and entanglement transitions following a quench or in the presence of a periodic drive.

The purpose of the current work is to investigate an important related feature of these systems. Namely, why the spectra of certain non-Hermitian Hamiltonians are entirely real in some parameter regimes. Note, this question cannot be addressed completely by invoking global symmetries. For example, pseudo-Hermiticity only guarantees that complex eigenvalues, if they appear, come in complex conjugate pairs [28,29]. Likewise, a so-called \mathcal{PT} -symmetric system, where \mathcal{P} and \mathcal{T} refer to parity and time reversal operators, respectively, has completely real eigenvalues only in the regime where all the energy eigenfunctions are also simultaneously eigenfunctions of the \mathcal{PT} operator [30–32] and the question remains as to what guarantees the latter. In fact, as discussed later, the models that we study in this work are not \mathcal{PT} -symmetric and, as such, \mathcal{PT} symmetry plays no role.

In this work we show that the combination of dynamical constraints imposed in the limit of large interaction along with global symmetries together can protect a “phase” where the spectrum is entirely real. We illustrate our idea with finite chains of the fermionic Hatano-Nelson (HN) and the non-Hermitian Su-Schrieffer-Heeger (SSH) models with nearest neighbor interaction.

An important ingredient in what follows is strong Hilbert space fragmentation in the limit of infinitely large interaction, where the Fock space breaks up into dynamically disjoint pieces whose number scales exponentially with the system size [33,34]. This phenomena is the focus of intense research at present in Hermitian systems, since it leads to nonergodicity and the ability to generate exotic nonequilibrium states [35–44].

Our main results are the following. (1) We show analytically that in the fragmented limit there are many-body similarity transformations that map the above non-Hermitian systems to Hermitian ones. Thus, in this limit, the spectra are real. In fact, fragmentation and real spectrum are both shown to be consequences of the same dynamical constraints which emerge in the limit of infinitely large interaction. (2) We show that the spectra persist to be real for arbitrarily large but finite interaction, provided the systems have sufficient global symmetry protection. These symmetries impose a hidden Hermiticity in those subspaces where the reality of the spectrum is not guaranteed by the fragmentation limit. Results (1) and (2) together imply that the spectra are real for interactions above finite critical values where the systems encounter many-body exceptional points. (3) We compute a local equal-time density-density fermionic correlation function and show that it can be used to detect the exceptional point location. Overall, our work provides the first analysis of the role of dynamical constraints in determining the spectrum of a non-Hermitian system.

The plan of the rest of the paper is as follows. In Sec. II, we discuss the role of HSF on the reality of the eigenspectra of the Hatano-Nelson model and demonstrate the presence of a “phase” with entirely real eigenvalues. This is followed by Sec. III, where analogous phenomena is discussed for the SSH model. Next, in Sec. IV, we discuss the behavior of the equal-time correlation function of the Hatano-Nelson model. Finally, we conclude in Sec. V. Some details of the calculations are elaborated in the Appendices.

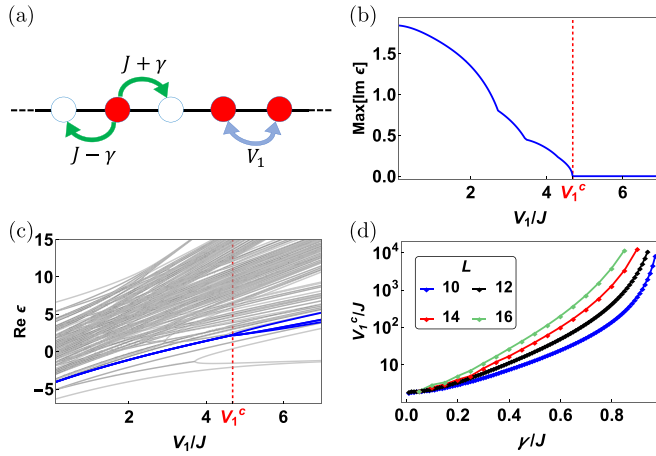


FIG. 1. (a) Schematic of Hatano-Nelson model with nonreciprocal hopping and nearest neighbor interaction V_1 . Filled sites are marked red. Panels (b) and (c) show the maximum imaginary and the real parts of the spectrum, respectively, as a function of V_1 , for system size $L = 10$ and $\gamma = 0.2J$. At V_1^c the system encounters a many-body exceptional point. For $V_1 < V_1^c$ complex conjugate pairs of eigenvalues first appear. In (c) the two eigenvalues which coalesce at the exceptional point are delineated in blue. (d) V_1^c diverges as $\gamma \rightarrow J$, and also with L .

II. HATANO-NELSON MODEL

A. Model

For pedagogical reason we demonstrate our principle in detail first for the HN model and argue later that the same holds for the SSH model. In terms of fermionic creation and annihilation operators (c_i^\dagger, c_i) at site i the HN Hamiltonian is

$$\mathcal{H}_{HN} = \sum_{i=1}^L [(J - \gamma)c_i^\dagger c_{i+1} + (J + \gamma)c_{i+1}^\dagger c_i + V_1 \hat{n}_i \hat{n}_{i+1}], \quad (1)$$

where $\hat{n}_i \equiv c_i^\dagger c_i$ is the number operator at site i , L is the system size, and $\gamma > 0$ is the nonreciprocal hopping parameter; see Fig. 1(a). We study the system at half filling with $\sum_i n_i = L/2$ and we impose (anti)periodic boundary condition for total particle number (even) odd. This choice ensures that the system is translationally invariant, as discussed below and in Appendix D. For the open boundary condition and $\gamma < J$ the problem is trivial because there is a one-body similarity transformation which makes \mathcal{H}_{HN} Hermitian [24]. As discussed in detail in the next section, \mathcal{H}_{HN} is pseudo-Hermitian, while its global symmetries are $\mathcal{G} = (\mathcal{P}\mathcal{C}, \mathcal{R})$ with $[\mathcal{H}_{HN}, \mathcal{G}] = 0$, where $(\mathcal{P}, \mathcal{C}, \mathcal{R})$ are parity, charge conjugation, and translation by one site, respectively. Furthermore, since integrability plays no role, our results are valid even in the presence of next-nearest neighbor interaction.

The spectral properties of \mathcal{H}_{HN} are summarized in Figs. 1(b)–1(d). Panels (b) and (c) show that, for $\gamma < J$, the spectrum is real for $V_1 > V_1^c$, a critical value. As shown in (c), at V_1^c one pair (or two pairs) of eigenvalues and eigenvectors coalesce at a many-body exceptional point and they become complex conjugate pairs for $V_1 < V_1^c$, as dictated by the pseudo-Hermiticity of \mathcal{H}_{HN} . Panel (d) shows that V_1^c

diverges as $\gamma \rightarrow J$ and also with system size L . Note, while these features were reported recently [45], the link between Hilbert space fragmentation with the reality of the spectrum, which is the focus of this work, has not been explored earlier.

B. Global symmetries

We mention two transformations which establish that the above Hamiltonian is pseudo-Hermitian. First, parity transformation \mathcal{P} , such that the site number $i \rightarrow (L - i + 1)$. Since this maps right hops to left hops and vice versa, we get $\mathcal{P}\mathcal{H}_{HN}\mathcal{P} = \mathcal{H}_{HN}^\dagger$. Second, particle-hole transformation \mathcal{C} , such that $\mathcal{C}c_i\mathcal{C} = (-1)^i c_i^\dagger$. Under this transformation, $c_i^\dagger c_{i+1} \rightarrow -c_i c_{i+1}^\dagger = c_{i+1}^\dagger c_i$ and $c_{i+1}^\dagger c_i \rightarrow c_i^\dagger c_{i+1}$. Thus the strengths of the right and the left hops are interchanged. The density-density interaction $n_i n_{i+1} \rightarrow (1 - n_i)(1 - n_{i+1})$. However, due to half filling, this term remains invariant when summed over all sites. Thus, at half filling, we get $\mathcal{C}\mathcal{H}_{HN}\mathcal{C} = \mathcal{H}_{HN}^\dagger$. However, by themselves these relations do not guarantee that, at large interaction V_1 , the energy eigenvalues are real. It is well known that pseudo-Hermiticity simply guarantees that complex eigenvalues, if they appear, come in complex conjugate pairs.

Combining these two relations one gets a symmetry of the Hamiltonian \mathcal{H}_{HN} , namely $\mathcal{P}\mathcal{C}$, since $(\mathcal{P}\mathcal{C})\mathcal{H}_{HN}(\mathcal{P}\mathcal{C}) = \mathcal{H}_{HN}$. It is due to this symmetry that some energy eigenvalues are doubly degenerate (the nondegenerate ones being eigenstates of $\mathcal{P}\mathcal{C}$) leading to situations when two pairs of eigenvalues coalesce at the exceptional point. In addition to this, \mathcal{H}_{HN} respects the translational symmetry \mathcal{R} [$i \rightarrow (i + 1)$ modulo L], which plays an important role in preserving the reality of the eigenspectrum for finite V_1 , as explained in a later section.

Note, in the absence of spin degrees of freedom, the Hamiltonian of Eq. (1) is trivially time reversal symmetric, with $\mathcal{T}\mathcal{H}_{HN}\mathcal{T} = \mathcal{H}_{HN}$. This implies that $(\mathcal{P}\mathcal{T})\mathcal{H}_{HN}(\mathcal{P}\mathcal{T}) = \mathcal{H}_{HN}^\dagger$. In other words, the model is not $\mathcal{P}\mathcal{T}$ -symmetric.

C. Limit of fragmentation

For large interaction, we keep terms to linear order in (J, γ) and ignore those of order $(J, \gamma)^2/V_1$ and smaller. This gives [46]

$$\mathcal{H}_{HN} \approx \mathcal{H}_{HN,f} = \sum_{i=1}^L [\hat{P}_i ((J - \gamma)c_i^\dagger c_{i+1} + (J + \gamma)c_{i+1}^\dagger c_i) \hat{P}_i + V_1 \hat{n}_i \hat{n}_{i+1}], \quad (2)$$

where the projector $\hat{P}_i \equiv 1 - (\hat{n}_{i-1} - \hat{n}_{i+2})^2$ ensures that the hopping is constrained, and is allowed only if the process does not change the total number of nearest neighbor occupations $\hat{N}_d \equiv \sum_i \hat{n}_i \hat{n}_{i+1}$.

The Hermitian version of $\mathcal{H}_{HN,f}$ has been shown to display strong Hilbert space fragmentation [37,38]. Since fragmentation is independent of whether the hopping mediated connectivity between the many-body Fock states is reciprocal or not, the non-Hermitian $\mathcal{H}_{HN,f}$ shows fragmentation as well. Below we prove that the dynamical constraints that give rise to fragmentation ensure the existence of a

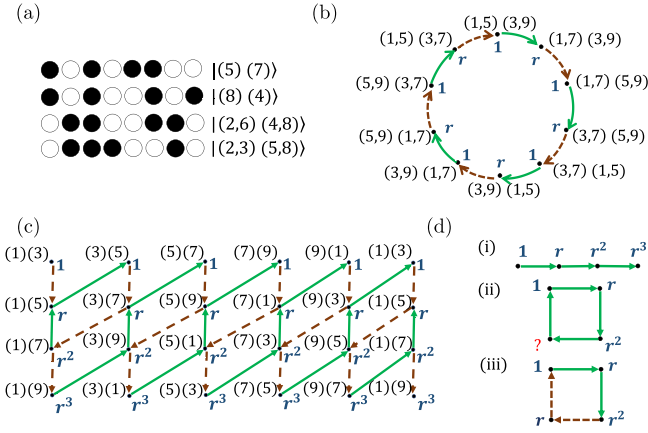


FIG. 2. (a) Examples of labeling many-body wave functions by the location of “defects.” Two nearest neighbor sites form a particle or a hole defect when they are both occupied or both unoccupied, respectively. The defect position is the location of the leftmost of the two sites. Panels (b) and (c) are examples of connectivities for $L = 10$, $N_d = 2, 1$, respectively; see text. Solid (green) and dashed (brown) arrows denote fermions hopping to the right and left, respectively. Reversing an arrow direction implies exchanging solid \leftrightarrow dashed. (d) Three examples of nonreciprocal hopping over four sites: (i) has open boundary, while (ii) and (iii) have periodic boundary conditions. $1, r, r^2$, etc. (in blue) in (b)–(d) are the scaling factors λ , such as in Eq. (3), of the wave functions next to them, which define the similarity transformation, wherever possible. In [(d)(ii)] one of the sites, indicated by a question symbol, cannot be scaled consistently. For a closed loop a similarity transformation is only possible if there are equal numbers of solid and dashed arrows while traversing the loop in a given direction, as in [(d)(iii)].

many-body similarity transformation that maps $\mathcal{H}_{HN,f}$ into a Hermitian form for $\gamma < J$.

D. Many-body similarity transformation

The first step of the proof is to label the many-body states. Traditionally, this is done using “spins and movers” [37,38,46]. Here we take a different strategy and we label them by “defects.” A “particle defect” and a “hole defect” are two occupied or two unoccupied nearest-neighbor sites, respectively. Due to half filling, particle and hole defects appear in pairs and their numbers are conserved, since $[\mathcal{H}_{HN,f}, \hat{N}_d] = 0$. Thus the Hilbert space factorizes into sectors with eigenvalue $N_d = 0, 1, \dots, L/2 - 1$.

All dynamically frozen (i.e., zero connectivity) states, which includes the $N_d = 0$ sector, have real energies. For $N_d \neq 0$ we label a defect position by the location of the leftmost of the two nearest-neighbor sites. Thus any state with $N_d = 1$ has label $|(i)(j)\rangle$, where i and j are locations of the particle and hole defect, respectively. Likewise, a state with $N_d = 2$ is labeled by $|(i_1, i_2)(j_1, j_2)\rangle$ and $N_d = n$ by $|(i_1, i_2, \dots, i_n)(j_1, j_2, \dots, j_n)\rangle$. Since the fermions are indistinguishable, permutations of i and of j imply the same state. Thus the state $|(5)(7)\rangle$ shown in Fig. 2(a) belongs to $N_d = 1$ and has a particle and a hole defect at sites $i = 5, 7$, respectively.

Due to half filling the defect locations are not arbitrary, but follow certain rules. (a) If two particle defects at i_1 and

i_2 are “adjacent,” then (i_1, i_2) can only be (odd, even) or (even, odd). The same applies for two “adjacent” hole defects. Here, adjacent does not imply defects located right next to one another. Two defects are adjacent if there is no third defect in between the two while traversing in one of the two directions. (b) If a particle defect at i_1 is adjacent to a hole defect at j_1 , then (i_1, j_1) can only be (even, even) or (odd, odd). One can verify that the wave functions in Fig. 2(a) satisfy these rules.

The second step is to determine the defect dynamics which, due to the constrained hopping, obey the following rules. (i) An allowed fermion hop changes i or j by ± 2 modulo L . (ii) Since second nearest neighbor hopping is absent, two defects cannot cross each other. It is shown in Appendix A that due to rules (i) and (ii) each sector of N_d breaks into an exponentially large number of disjoint subsectors, i.e., fragments, that scale as e^{N_d} [34].

The third step is to establish the constrained hopping induced connectivity between the many-body wave functions within each nontrivial subsector. There is no general pattern for these connectivities and they need to be worked out case by case, even though the proof below holds for all the connectivities. To show a few examples, Fig. 2(b) is the connectivity for $L = 10$, $N_d = 2$ with $(i_1, i_2)(j_1, j_2) = (\text{odd}, \text{odd})(\text{odd}, \text{odd})$, while Fig. 2(c) is for $L = 10$, $N_d = 1$ with $(i)(j) = (\text{odd})(\text{odd})$. The dashed and solid arrows denote fermions hopping to the left and right (amplitudes $J_{1,2} \equiv J \mp \gamma$), respectively. Reversing an arrow implies $J_1 \leftrightarrow J_2$. A fermion hopping left can result in either a particle defect moving left, i.e., $i \rightarrow (i - 2) \bmod L$, or a hole defect moving right, i.e., $j \rightarrow (j + 2) \bmod L$. Thus each connectivity diagram can be viewed as a single particle hopping in the abstract space of many-body wave functions in a nonreciprocal manner.

The fourth and final step of the proof is to establish the existence of the similarity transformation in each subsector. For pedagogical reason we first consider a few examples of nonreciprocal hopping of a single particle in a four-site system. Figure 2(d)(i) is a linear chain with open boundary condition. This can be mapped to a Hermitian form for $\gamma < J$ by the scaling

$$|i\rangle \rightarrow \lambda_i |i\rangle, \quad \langle i| \rightarrow (1/\lambda_i) \langle i|, \quad (3)$$

where $\lambda_i = 1, r, r^2, r^3$, for $i = 1, \dots, 4$, respectively, and $r \equiv \sqrt{J_2/J_1}$ [24]. However, for periodic boundary condition, as in Fig. 2(d)(ii), the transformation will not work since the new link 4 -1 of the closed loop cannot be made Hermitian. This exemplifies that finding similarity transformations is nontrivial where the connections form closed loops, which is precisely our case as seen in, e.g., Figs. 2(b) and 2(c). Now consider Fig. 2(d)(iii), which is also a closed loop, but where the hops are J_2, J_2, J_1, J_1 moving clockwise. In this case, once again, a similarity mapping exists, with $\lambda_i = 1, r, r^2, r$, respectively. This example illustrates the crucial property that a closed loop with *equal* number of J_1 and J_2 hops, while traversing along a direction, can be mapped to a Hermitian form. This is because a J_2 link requires an additional scaling of r for the second site compared to the first, which is compensated by a J_1 link which requires a $1/r$ scaling. This is exactly the case for the connectivities of Figs. 2(b) and 2(c), where the scalings associated with the wave functions are marked in blue. Additional examples of such scalings are discussed

in Appendix B. We prove below that *all* the connections of $\mathcal{H}_{HN,f}$ are such that each and every possible loop has this property.

Starting from any $|(i_1, i_2, \dots, i_n)(j_1, j_2, \dots, j_n)\rangle$, a closed loop is obtained in three basic ways.

(1) If one or more of the site indices change as, say, $i \rightarrow i' \rightarrow i''$ and so on, and then reverse the path to go back to i , while obeying the rules (i) and (ii). Since the reverse of a J_1 hop is a J_2 hop, and vice versa, traversing the loop along one direction will necessarily have an equal number of J_1 and J_2 hops. The loop (1)(7) \rightarrow (1)(5) \rightarrow (3)(5) \rightarrow (3)(7) \rightarrow (1)(7) in Fig. 2(c) is an example.

(2) If a defect does not retrace its path, but moves across the chain, traversing L sites, and gets back to its original position using the periodic boundary condition. However, according to rule (ii) this can happen only if all other defects perform the same circular motion in the same direction and regain their original positions, each having traversed L sites. Since a particle-defect moving to the right is a J_2 hop, while a hole defect moving to the right is a J_1 hop, and since there are an equal number of particle and hole defects, this loop, too, will have an equal number of J_1 and J_2 hops. Starting from state (1)(3) on the left side of Fig. 2(c) and ending again at (1)(3) on the right side of the figure is an example of such a loop.

(3) In some cases, such as in Fig. 2(b), it is possible for the defects to exchange positions such that $i_1 \rightarrow i_2 \rightarrow i_3 \cdots \rightarrow i_n \rightarrow i_1$ and $j_1 \rightarrow j_2 \rightarrow j_3 \cdots \rightarrow j_n \rightarrow j_1$. In this case a loop is completed by permuting the indices, while the defects neither retrace their paths nor complete the circle. Here the sum of the sites traversed by all the particle defects is L and the same is true for all the hole defects and they are along the same direction. Thus, again here, the loop has an equal number of J_1 and J_2 hops.

This completes the proof that $\mathcal{H}_{HN,f}$ can be mapped into a Hermitian form for $\gamma < J$; this feature guarantees the reality of eigenspectrum of $\mathcal{H}_{HN,f}$ in this limit.

E. Finite V_1^c and symmetry protection

The above conclusion is not sufficient for our purpose once V_1 is large but finite. To understand why, consider two eigenstates of $\mathcal{H}_{HN,f}$ from the same subsector of \hat{N}_d . Measuring energies from the average eigenvalue, the subsystem has the structure

$$\mathcal{H}_{\text{eff}} = \begin{pmatrix} l & m_1 + m_2 \\ m_1 - m_2 & -l \end{pmatrix},$$

with eigenvalues $\pm \sqrt{l^2 + m_1^2 - m_2^2}$. Since $m_{1,2} \sim \mathcal{O}((J, \gamma)^2/V_1)$ or smaller, for finite l the reality of the eigenvalues is guaranteed for V_1 sufficiently large. But, this argument fails in the case of degeneracy when $l = 0$. Nevertheless, the reality of the spectrum can still be protected if the two degenerate states are connected by a symmetry \mathcal{G} of the full Hamiltonian \mathcal{H}_{HN} , which squares to identity in the degenerate subspace, as we show below.

Let $|\psi\rangle$ and $|\phi\rangle$ represent two degenerate right eigenstates of $\mathcal{H}_{HN,f}$ connected by a symmetry \mathcal{G} of both $\mathcal{H}_{HN,f}$ and \mathcal{H}_{HN} , i.e., $|\phi\rangle = \mathcal{G}|\psi\rangle$. The corresponding left eigenstates are $\langle\langle\psi|$ and $\langle\langle\phi| = \langle\langle\psi|\mathcal{G}^\dagger$. Further, let us assume

that $\mathcal{G}^2|\psi\rangle = |\psi\rangle$ and $\mathcal{G}^2|\phi\rangle = |\phi\rangle$. The off-diagonal matrix elements are seen to be equal as follows:

$$\begin{aligned} \langle\langle\psi|\mathcal{H}_{HN}|\phi\rangle &= \langle\langle\phi|\mathcal{G}\mathcal{H}_{HN}\mathcal{G}|\psi\rangle \\ &= \langle\langle\phi|\mathcal{H}_{HN}\mathcal{G}^2|\psi\rangle \\ &= \langle\langle\phi|\mathcal{H}_{HN}|\psi\rangle. \end{aligned} \quad (4)$$

Since the eigenvectors of $\mathcal{H}_{HN,f}$ can be chosen to be real when its eigenvalues are real, these matrix elements are also real. This implies that the full Hamiltonian \mathcal{H}_{HN} effectively has a Hermitian structure within this degenerate subspace. The degeneracy of the two states $|\psi\rangle$ and $|\phi\rangle$ at the level of $\mathcal{H}_{HN,f}$ is lifted by $\delta\mathcal{H}_{HN} = \mathcal{H}_{HN} - \mathcal{H}_{HN,f}$ in a Hermitian manner at most. This leads to level repulsion which is opposite to what is required for two eigenstates to coalesce. This also implies that eigenstates, or their linear combinations, that are related by symmetry of the type of \mathcal{G} cannot coalesce. Thus there will be a finite range of V_1 for which the spectrum of \mathcal{H}_{HN} would be real, until one (or two) pair(s) of eigenstates, not related by any symmetry (of the type of \mathcal{G}) coalesce at an exceptional point. We illustrate this using one concrete example in Appendix C.

As discussed in Appendix D, the above symmetry protection can be destroyed by a choice of boundary condition that breaks translation symmetry. In this case one has complex eigenvalues for any finite value of V_1 , even though the spectrum is real in the fragmented limit.

We estimate $l \sim \sqrt{J^2 - \gamma^2}/e^{cL}$ by the average level spacing of a subsector, where the constant $c > 0$ depends on the subsector size. Empirically, we find that, for the pair that coalesce, m_1 is at least one order of magnitude smaller than m_2 , while $m_2 \propto V_1^{-\alpha}(J^2 - \gamma^2)^{-\beta/2}$, where the exponents (α, β) are L dependent. This implies that $V_1^c \sim J e^{cL/\alpha}/[1 - (\gamma/J)^2]^{(\beta+1)/(2\alpha)}$. Thus, as shown in Fig. 1(d), V_1^c diverges exponentially with L and as a power law with an L -dependent exponent for $\gamma \rightarrow J$.

Note, in passing, that for certain values of L the two coalescing levels at V_1^c are each doubly degenerate, so that below V_1^c there are two pairs of complex conjugate eigenvalues. This degeneracy is related to \mathcal{PC} invariance.

III. GENERALIZATION TO THE NON-HERMITIAN SU-SCHRIEFFER-HEEGER MODEL

A. Model

Next we discuss the non-Hermitian interacting SSH model as one possible generalization of the concept presented in the previous section. We consider a fermionic SSH chain with left (right) intracellular hopping $J_1 = J - \gamma_1$ ($J_2 = J + \gamma_1$), left (right) intercellular hopping $K_1 = K - \gamma_2$ ($K_2 = K + \gamma_2$), and a nearest neighbor interaction V_1 , as shown in Fig. 3(a). The Hamiltonian of the system reads

$$\begin{aligned} \mathcal{H}_{\text{SSH}} = & \sum_{i=1}^{L/2} [J_1 c_{2i-1}^\dagger c_{2i} + J_2 c_{2i}^\dagger c_{2i-1} \\ & + K_1 c_{2i}^\dagger c_{2i+1} + K_2 c_{2i+1}^\dagger c_{2i}] + \sum_{i=1}^L V_1 \hat{n}_i \hat{n}_{i+1}. \end{aligned} \quad (5)$$

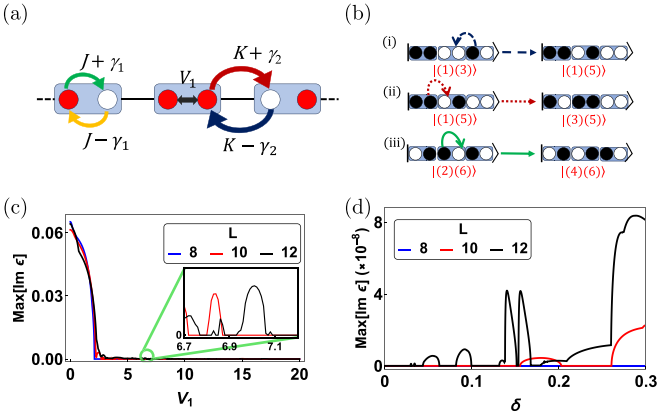


FIG. 3. (a) Schematic of the interacting SSH model with nonreciprocal intra- and intercellular hops and nearest neighbor interaction V_1 . The blue boxes indicate one unit cell of the SSH chain and the filled sites are marked in red. (b) Defects at odd site can only move by an intercellular hop [blue dashed and red dotted in (i) and (ii)], while defects at even site can move by an intracellular hop [green solid in (iii)]. (c) Variation of the maximum imaginary part of the eigenvalues with the interaction strength V_1 for three system sizes $L = 8, 10, 12$ corresponding to $\gamma_1 = \gamma_2 = 0.1$, $J = 0.9$, and $K = 1.0$. For all the system sizes, beyond a certain interaction strength, the imaginary parts of the eigenvalues become zero within numerical precision. The inset shows islands at $V_1 < V_1^c$ (for instance, $V_1^c = 23.8$ for $L = 10$) for $L = 10$ (red) and $L = 12$ (black), where the imaginary part is finite, but orders of magnitudes smaller than the real part. (d) Variation of the maximum imaginary part of the eigenvalues with $\delta = K - J$ for three system sizes $L = 8, 10, 12$ with $\gamma_1 = \gamma_2 = 0.1$, $K = 1.0$, and $V_1 = 1000$. The presence of a critical value of δ ($\delta_c = 0.156$ for $L = 10$, for example), below which the spectrum is completely real is seen. Also, the value of δ_c at a given V_1 reduces with increase in system size. See text for details.

Each unit cell is composed of two nonequivalent sites $2i - 1$ and $2i$ so that there are L sites in total. The nearest neighbor interaction V_1 does not distinguish between the two nonequivalent sites. The non-Hermiticity of \mathcal{H}_{SSH} arises due to the nonreciprocal intracellular and intercellular hoppings.

As we show here, there exists a one-body similarity transformation by virtue of which, for any parameter set $(J, K, \gamma_1, \gamma_2)$, γ_1 can be made equal to γ_2 , while keeping different values of J and K . To do so, we scale the particle creation and annihilation operator on every odd site by

$$c_{2j-1}^\dagger \rightarrow \lambda c_{2j-1}^\dagger, \quad c_{2j-1} \rightarrow \frac{1}{\lambda} c_{2j-1},$$

respectively. In terms of these transformed operators, the Hamiltonian reads

$$\begin{aligned} \mathcal{H}_{SSH} = & \sum_{i=1}^{L/2} [\tilde{J}_1 c_{2i-1}^\dagger c_{2i} + \tilde{J}_2 c_{2i}^\dagger c_{2i-1} \\ & + \tilde{K}_1 c_{2i}^\dagger c_{2i+1} + \tilde{K}_2 c_{2i+1}^\dagger c_{2i}] + \sum_{i=1}^L V_1 \hat{n}_i \hat{n}_{i+1}, \end{aligned} \quad (6)$$

where $\tilde{J}_1 = \tilde{J} + \tilde{\gamma}_1 = \lambda J_1$, $\tilde{J}_2 = \tilde{J} - \tilde{\gamma}_1 = J_2/\lambda$, $\tilde{K}_1 = \tilde{K} + \tilde{\gamma}_2 = K_1/\lambda$, and $\tilde{K}_2 = \tilde{K} - \tilde{\gamma}_2 = \lambda K_2$. Choosing

$$\lambda = \sqrt{\frac{J + K + \gamma_2 - \gamma_1}{J + K - \gamma_2 + \gamma_1}},$$

one gets $\tilde{\gamma}_1 = \tilde{\gamma}_2$ in this transformed frame, while $\tilde{J} \neq \tilde{K}$. For our numerical results, we choose our parameter set to obey this and vary $\delta = K - J$, without any loss of generality.

We consider the chain at half filling, $\sum_i n_i = L/2$, with (anti)periodic boundary condition for (even) odd $L/2$. Figure 3(c) shows that, in this case too, there is a strength of the nearest neighbor interaction, V_1^c , above which the spectrum is completely real within numerical precision. For $V_1 < V_1^c$, islands appear in the spectrum where the imaginary part is orders of magnitude smaller than the real part of the eigenvalues. The islands progressively shorten in height before hitting zero within numerical precision at V_1^c . The inset of Fig. 3(c) shows such islands. The value of this interaction strength is seen to increase with system size as well as with δ .

B. Fragmentation and similarity transformation

We consider the large V_1 limit, $V_1 \gg J, K, \gamma_1, \gamma_2$, and focus on the first-order effective Hamiltonian

$$\begin{aligned} \mathcal{H}_{SSH,f} = & \sum_{i=1}^{L/2} \left[\hat{P}_{2i} (J_1 c_{2i-1}^\dagger c_{2i} + J_2 c_{2i}^\dagger c_{2i-1}) \hat{P}_{2i} \right. \\ & + \hat{P}_{2i+1} (K_1 c_{2i}^\dagger c_{2i+1} + K_2 c_{2i+1}^\dagger c_{2i}) \hat{P}_{2i+1} \\ & \left. + V_1 \sum_{i=1}^L \hat{n}_i \hat{n}_{i+1} \right], \end{aligned} \quad (7)$$

where $\hat{P}_i = 1 - (\hat{n}_{i-2} - \hat{n}_{i+1})^2$ is a projector that only allows those hops which preserve the number of nearest neighbor pairs (defects), $N_d = \sum_i n_i n_{i+1}$. It is useful to remember here that a particle defect refers to two particles sitting on neighboring sites and a hole defect refers to two neighboring vacant sites. In addition, since a particle hop changes the position of a defect by ± 2 modulo L sites, therefore the number of defects at odd sites ($N_{d,\text{odd}} = \sum_i n_i n_{i+1}$) and even sites ($N_{d,\text{even}} = \sum_i n_i n_{i+1}$) are individually conserved by $\mathcal{H}_{SSH,f}$. Here, single (double) prime implies sum over odd (even) sites only. It is easy to see now that these constraints are similar to those which appear in the Hatano-Nelson model in the large V_1 limit. Since the connectivity of states in the Hilbert space does not depend on the hopping strengths (as long as they are much smaller than V_1), therefore $\mathcal{H}_{SSH,f}$ also exhibits strong Hilbert space fragmentation in spite of having different intercellular and intracellular hoppings.

In addition, it is important to note the following. (i) At half filling, the number of particle defects at the odd sites is equal to the number of hole defects at odd sites and the same holds true for defects at even sites. (ii) A defect at an odd site can only move by an intercellular hop and a defect at an even site can only move by an intracellular hop [Fig. 3(b)]. (iii) Two defects cannot cross each other.

It remains to understand whether the similarity transformation goes through in the fragmented limit. For this purpose, we need to label the states first. The labeling scheme is similar to

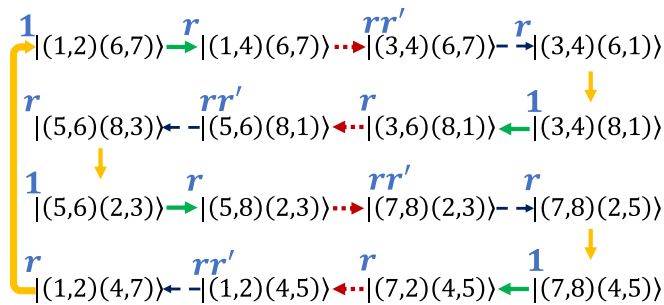


FIG. 4. Connectivity diagram of $\mathcal{H}_{SSH,f}$ in Fock space showing type (2) connectivity in which the defects traverse through the entire chain to return to their original configuration. Solid green and yellow arrows refer to right and left intracellular hops, respectively, while red dotted and blue dashed arrows refer to right and left intercellular hops, respectively. See text for details.

that used in the case of Hatano-Nelson model. Thus, in the $N_d = 1$ sector, $|i(j)\rangle$ denotes a state having a particle defect at site i and a hole defect at site j . Similarly, in the $N_d = 2$ sector, a state is labeled as $|(i_1, i_2)(j_1, j_2)\rangle$ and a state in the $N_d = n$ sector is $|(i_1, i_2, \dots, i_n)(j_1, j_2, \dots, j_n)\rangle$.

Next, it is again useful to remember here that for the similarity transformation to be consistent along a closed loop (in Fock space), the number of right nonreciprocal hops should be equal to the number of left nonreciprocal hops along the loop. Since, in this particular case, the intercellular and intracellular hops are individually nonreciprocal, this criterion translates to having an equal number of right and left intercellular hops and an equal number of right and left intracellular hops separately along any closed loop. To check whether this is the case, we again consider the three ways by which a state $|(i_1, i_2, \dots, i_n)(j_1, j_2, \dots, j_n)\rangle$ can close on to itself in Fock space.

(1) *The defects retrace their path.* In this case, one or more defects hop following $i \rightarrow i' \rightarrow i'' \rightarrow \dots$ and then retrace their path to return to the original configuration and close the loop. Since a right intercellular (intracellular) hop will necessarily require a left intercellular (intracellular) hop for its reversal, therefore, in this case, it trivially holds that a closed loop will have an equal number of right and left intercellular (intracellular) hops.

(2) *The defect moves across the chain making L hops and returns to its original position using the periodic boundary condition.* Due to rule (iii) above, this implies that all other defects would also have to return to their initial positions after going across the chain in the same direction. Each such defect will have to make L hops across the chain. From rules (i) and (ii), this implies that there will be an equal number of particle and hole defects undergoing intercellular (intracellular) hops in the same direction. Since a particle defect hopping to the right is equivalent to a particle hopping to the right and a hole defect hopping to the right is equivalent to a particle hopping to the left, this suggests that, in this case too, there will be an equal number of right and left intercellular hops and an equal number of right and left intracellular hops separately along a closed loop. This is shown in Fig. 4.

(3) *The defects permute their positions to reach the initial configuration.* In this case, a sequence of defects exchange

their positions as $i_1 \rightarrow i_2 \rightarrow i_3 \rightarrow \dots \rightarrow i_n \rightarrow i_1$ and $j_1 \rightarrow j_2 \rightarrow j_3 \rightarrow \dots \rightarrow j_n \rightarrow j_1$ to reach the initial state and complete the loop. Thus the sum of the sites traversed by all the particle defects is L and the same is true for all the hole defects. However, this type of connectivity is only possible if all the defects are present either on the odd sites or on the even sites. If the defects are on odd (even) sites and the motion is along the counterclockwise direction, then all the hops of the particle defects will be of the type K_2 (J_2), while those of the hole defects will be of the type K_1 (J_1). Thus, here too, there will be an equal number of $K_{1,2}$ hops and no $J_{1,2}$ hop or vice versa.

Thus a consistent similarity transformation can always be carried out along any closed loop with each right and left intracellular (intercellular) hop being scaled by a factor r (r') and $1/r$ ($1/r'$), respectively, where $r = \sqrt{\frac{J_2}{J_1}}$ and $r' = \sqrt{\frac{K_2}{K_1}}$.

C. Symmetry protection

In this section, we discuss the protection of the real eigenvalues once we move out of the limit of fragmentation $\mathcal{H}_{SSH,f}$ by considering large, but finite, V_1 . As discussed for the HN model, the nondegenerate eigenvalues are guaranteed to stay real once V_1 is finite, while the degenerate ones are not. In the HN model we found that the degenerate subspaces are symmetry protected which enforces Hermiticity in these subspaces. The case of the SSH model is more complex because, due to period doubling with $J \neq K$, translations by an odd number of sites are no longer symmetry operations. Thus we find certain pairs of degenerate eigenvalues in the fragmented limit which are not symmetry connected. These pairs are symmetry connected only if $J = K$ when the full translation symmetry of the chain is restored, i.e., in the limit of the HN model. As expected, we find that in such projected non-symmetry connected two-dimensional subspaces the effective Hamiltonian is non-Hermitian with the structure

$$\mathcal{H}_{\text{eff}} = \begin{pmatrix} l & m_1 + m_2 \\ m_1 - m_2 & -l \end{pmatrix},$$

with $m_{1,2} \neq 0$. However, if we define $\delta \equiv (K - J)$ as the deviation from the HN limit, we are guaranteed that the non-Hermitian component $m_2 \rightarrow 0$ as $\delta \rightarrow 0$. Thus, for V_1 sufficiently large (larger than V_1^c of the HN model), there is a finite critical value δ_c below which $m_1 > m_2$ for all such non-symmetry connected degenerate pairs of eigenvalues, which guarantees that the eigenvalues stay real even if the subspace is non-Hermitian. This is shown in Fig. 3(d) for $L = 8, 10, 12$. The value of δ_c is seen to decrease with an increase in system size for a given value of V_1 . Beyond δ_c , islandlike features again emerge suggesting that the behavior of m_2/m_1 is non-monotonic as a function of δ .

IV. CORRELATION FUNCTION AND DETECTION OF AN EXCEPTIONAL POINT

In this section, we study the time evolution of a correlation function which, in principle, can be measured to identify the location of a many-body exceptional point. We choose the Hatano-Nelson model for this purpose. One such example is $\chi(t) = \langle \psi(t) | \hat{N}_d | \psi(t) \rangle / L$ starting from a random Fock

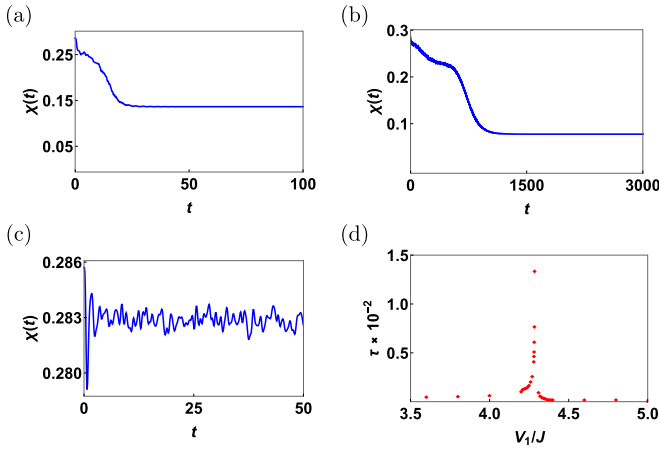


FIG. 5. (a)–(c) Time evolution of the correlation function $\chi(t)$ for $V_1 = 3J$, $4.285J$, and $6J$, respectively, for $L = 14$ and $\gamma = 0.2J$. In (b) the system is very close to the exceptional point at $V_1^c \approx 4.2863$. (d) Variation of the relaxation timescale τ with V_1 showing a one-sided divergence as $V_1 \rightarrow V_1^c$ from below.

state $|\psi(0)\rangle = \sum_m c_m |\phi_m\rangle$, expanded in the basis of the right eigenvectors $|\phi_m\rangle$ of \mathcal{H}_{HN} . The time-evolved wave function, suitably normalized to account for the non-Hermiticity of \mathcal{H}_{HN} , is

$$|\psi(t)\rangle = \frac{e^{-i\mathcal{H}_{HN}t/\hbar}|\psi(0)\rangle}{\|e^{-i\mathcal{H}_{HN}t/\hbar}|\psi(0)\rangle\|} = \frac{\sum_m c_m(t)|\phi_m\rangle}{\sqrt{\sum_{m,n} c_m^*(t)c_n(t)\langle\phi_m|\phi_n\rangle}},$$

where $c_m(t) = c_m e^{-i\epsilon_m t/\hbar}$.

Figure 5, panels (a)–(c), shows the time evolution of $\chi(t)$ for V_1 less than, nearly equal to, and greater than V_1^c , respectively, for the HN model. For $V_1 < V_1^c$ the time evolution is dominated by the eigenvalue with the largest imaginary component. Consequently, after a timescale $\tau \sim 1/\max[\text{Im } \epsilon]$, the correlation function attains a steady state value $\chi(t \gg \tau) \sim 1/L \langle \phi_m^* | \hat{N}_d | \phi_m^* \rangle$, where $|\phi_m^*\rangle$ is the eigenvector with the largest $\text{Im } \epsilon$. This implies that τ diverges as $V_1 \rightarrow V_1^c$ from below, as seen in Fig. 5(d). For $V_1 \geq V_1^c$ all the eigenvalues are real and the system quickly attains a diagonal ensemble and $\chi(t)$ fluctuates about an average value $\chi(t \gg \tau) \sim 1/L \sum_m |c_m|^2 \langle \phi_m | \hat{N}_d | \phi_m \rangle$ [47,48], implying that the peak of $\tau(V_1)$ in Fig. 5(d) is one sided. This peak can be used to detect the exceptional point.

V. DISCUSSION

In this work, we have studied the Hatano-Nelson and the Su-Schrieffer-Heeger models with nonreciprocal hops and nearest neighbor interactions. We have shown that these models provide two examples of a class of non-Hermitian systems which have a “phase” with an entirely real spectrum for sufficiently large interactions.

We note that none of these models have \mathcal{PT} symmetry. Thus the generic expectation in the existing literature for the existence of real eigenvalues in the presence of such symmetry is not applicable to the present models. Our work explicitly points out that the presence of global symmetries cannot, by itself, explain the reality of eigenspectrum of the models at large interaction strength.

In contrast, as we show in this work, such a phase with entirely real eigenspectrum is a consequence of two ingredients. First, the dynamical constraints in the infinitely large interaction limit which also fragments the Hilbert space of the models. This Hilbert space fragmentation leads to restriction on the matrix elements of the Hamiltonian between Fock states and, as we show, allows for an existence of a many-body similarity transformation, which allows us to prove the reality of the eigenspectrum in this limit. Second, moving away from the fragmented limit, we show that the presence of global symmetries allows one to retain the reality of eigenspectrum up to a critical interaction strength. The effective Hamiltonian between two states related by such symmetries (and which are therefore degenerate in the limit of large V) can be shown to be Hermitian for finite $V \leq V_c$; this allows for persistence of real eigenvalues until a critical interaction strength is reached. Interestingly, this mechanism seems to be effective even when such symmetries are weakly broken as seen from the analysis of the SSH model. Thus our work points out the role of HSF for the presence of a real eigenspectrum; to the best of our knowledge, such application of HSF in the context of non-Hermitian system has not been pointed out earlier.

In addition, we also provide a method of detection of the first exceptional point in these systems. Our analysis indicates that time taken by an equal-time correlator of such a system to reach its steady state value following a quench diverges at the first exceptional point. This observation, which only relies on the presence of an infinitesimal complex component of a pair of eigenvalues at this point, provides a link between the presence of exceptional points and the behavior of experimentally measurable equal-time correlation functions in such non-Hermitian systems.

To summarize, we reveal a deep link between the physics of fragmentation and the property of the real spectrum of an interacting non-Hermitian system. This link is worth investigating in the future to identify and construct other systems belonging to this class. We also propose a method to detect many-body exceptional points by studying the time required for a correlation function to reach its steady state value.

ACKNOWLEDGMENTS

The authors thank D. Sen for several comments. I.P. is thankful to M. Haque for insightful discussions. S.G. acknowledges the financial support provided by CSIR, India through File No. 09/080(1133)/2019-EMR-I. K.S. thanks DST, India for support through SERB Project No. JCB/2021/000030.

APPENDIX A: ARGUMENT FOR FRAGMENTATION

In Fig. 6, we plot the absolute difference, $\Delta_n = |\varepsilon_n - \varepsilon_n^f|$, between the energy eigenvalues ε_n of the exact Hamiltonian \mathcal{H}_{HN} and ε_n^f of the fragmented Hamiltonian $\mathcal{H}_{HN,f}$. We take $L = 8$ with anti-PBC. It can be seen that, as the nearest neighbor interaction V_1 increases, the spectrum of \mathcal{H}_{HN} approaches that of $\mathcal{H}_{HN,f}$. This implies that, in the large V_1 limit, $\mathcal{H}_{HN,f}$ gives the leading order description of \mathcal{H}_{HN} .

Next, we revisit the argument of why the constrained hopping of $\mathcal{H}_{HN,f}$ in Eq. (2) of the main text leads to strong

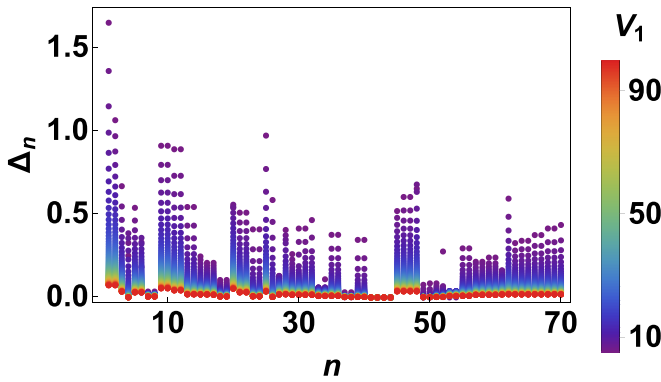


FIG. 6. Variation of the difference between the eigenvalues of \mathcal{H} and that of $\mathcal{H}_{HN,f}$ with V_1 for $L = 8$ with anti-PBC. As V_1 increases, $\mathcal{H}_{HN,f}$ increasingly becomes a better approximation to \mathcal{H}_{HN} . See text for details.

Hilbert space fragmentation. For the Hermitian case the argument can be found in the literature in terms of the mapping to “spins and movers” [37]. Since the argument is based in Fock space, it is valid as well for nonreciprocal hopping. Below we reconstruct the argument in terms of “particle and hole defects.”

As already outlined in the main text, due to half filling the defect locations follow certain rules. (a) If two particle defects at i_1 and i_2 are “adjacent,” then (i_1, i_2) can only be (odd, even) or (even, odd). The same applies for two adjacent hole defects. Two defects are adjacent if there is no third defect in between the two while traversing either clockwise or counterclockwise. (b) If a particle defect at i_1 is adjacent to a hole defect at j_1 , then (i_1, j_1) can only be (even)(even) or (odd)(odd).

Also, the defect dynamics, due to the constrained hopping, obey the following rules. (i) An allowed fermion hop changes i or j by ± 2 modulo L . (ii) Since second nearest neighbor hopping is absent, two defects cannot cross each other.

Due to rule (ii) two configurations in which the sequence of the defects are not cyclically related can never be connected by $\mathcal{H}_{HN,f}$ and hence they belong to two different fragments. Thus each fragment can be labeled by the sequence in which the defects appear while moving, say, from site 1 to L of the chain. As an example consider the sector $N_d = 3$. The wave functions have three particle defects and three hole defects. Note that the sequences need to obey rules (a) and (b) mentioned above. Moreover, due to rule (i), a defect on an odd (even) site always stays on an odd (even) site. There are eight possible different sequences that can be designated as

$$\begin{aligned} &(p_e, h_e, p_e, h_e, p_e, h_e), & (p_e, h_e, p_e, p_o, h_o, h_e), \\ &(p_e, p_o, p_e, h_e, h_o, h_e), & (p_o, p_e, h_e, p_e, h_e, h_o), \\ &(p_o, h_o, p_o, p_e, h_e, h_o), & (p_o, p_e, p_o, h_o, h_e, h_o), \\ &(p_e, p_o, h_o, p_o, h_o, h_e), & (p_o, h_o, p_o, h_o, p_o, h_o), \end{aligned}$$

where $p_{o/e}$ implies a particle defect on an odd (even) site and $h_{o/e}$ implies a hole defect on an odd (even) site. Thus, by suitably inserting hole defects, each of the three particle defects can be put either on an odd or on an even site. This implies 2^{N_d} distinct fragments. In practice, in between a p_e and a p_o one can put an even number, including zero, of hole

defects, and in between two p_e one can put an odd number of hole defects. This last flexibility makes the actual number of fragments more than 2^{N_d} for L and N_d large enough. Thus 2^{N_d} is a lower bound, which nevertheless shows that the number of fragments proliferate exponentially with the system size.

Next we enumerate the size of the largest fragment in the symmetry sector with $N_d = L/4$ defects. Consider a seed state with all the particle defects p to the left, followed by all the hole defects h and then pairs of filled and empty sites denoted by R ($R \equiv \bullet\circ$). This configuration has the form

$$\underbrace{(p, p, \dots)}_{N_d \text{ times}}, \underbrace{(h, h, \dots)}_{N_d \text{ times}}, \underbrace{(R, R, \dots)}_{P \text{ times}}.$$

Since N_d consecutive particle defects require $(N_d + 1)$ particles and N_d consecutive hole defects require $(N_d + 1)$ holes, while the remaining particle/holes are in pairs, the number of pairs is $P = L/2 - (N_d + 1)$. Under the action of $\mathcal{H}_{HN,f}$ a particle from R can “diffuse” into the sequence of hole defects. However, it needs to be accompanied by a hole as well, in order to maintain the number N_d of hole defects. The same is true for diffusion into the sequence of particle defects. For instance,

$$|\bullet\bullet\bullet\bullet\circ\circ\circ\circ\bullet\circ\rangle \rightarrow |\bullet\bullet\bullet\bullet\circ\circ\circ\circ\bullet\circ\rangle.$$

In other words, only pairs diffuse under the constrained hopping. The size of the fragment is given by the number of distinct wave functions that can be created from this seed state through pair diffusion. Since P pairs can be put in $2N_d$ intermediate positions in between the defects, and since translation of a given configuration by two sites also generates new configurations (note, defects can move only by two sites), the size of the largest fragment is

$$N_f = \frac{L}{2} \binom{2N_d + P - 1}{P} = \frac{L}{2} \binom{3L/4 - 2}{L/4 - 1}.$$

On the other hand, the total size of the symmetry sector with N_d defects is [38]

$$N_s = 2 \binom{L/2}{L/4} \binom{L/2 - 1}{L/4}.$$

In the limit of large chain length L , this implies that the ratio $\lambda \equiv N_f/N_s \approx (0.8)^L$, which vanishes exponentially with the system size. In other words, even the largest fragment samples only a vanishing portion of the total possible states. This establishes strong Hilbert space fragmentation.

APPENDIX B: MORE ON CONNECTIVITY DIAGRAMS AND SIMILARITY TRANSFORMATION

In this section, we provide an illustration of the similarity transformation in a simple case and explicit examples of the three possible types of closed loops as mentioned in the main text.

To begin with, we consider a chain of length $L = 6$ having three fermions with PBC. We focus on the $N_d = 1$ sector and since the Hamiltonian $\mathcal{H}_{HN,f}$ changes the positions of the hole and the particle defects by $\pm 2 \pmod{L}$ only, we consider the (odd)(odd) and the (even)(even) sectors separately. The basis states for the (odd)(odd) sector are enumerated

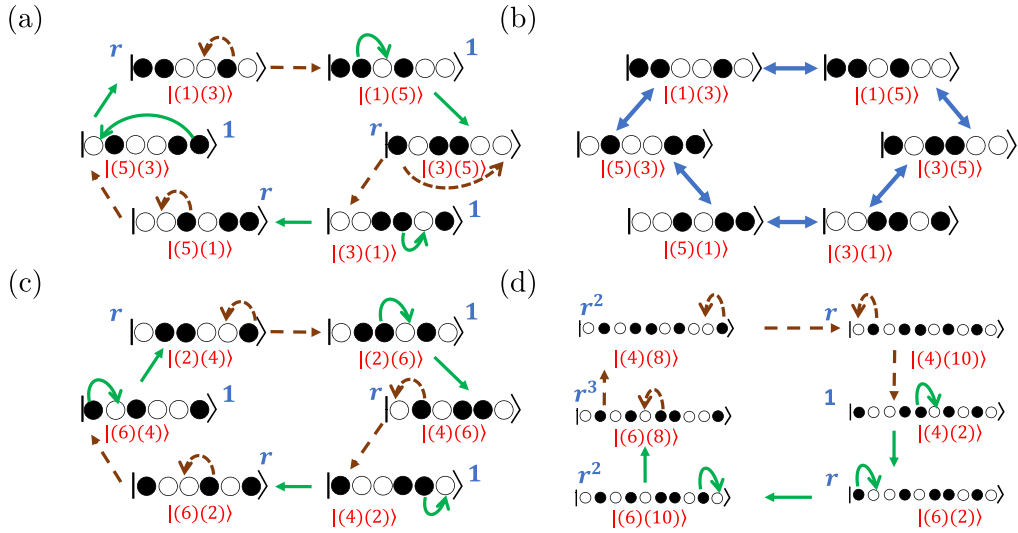


FIG. 7. (a) Connectivity diagram corresponding to $\mathcal{H}_{HN,f}^{\text{odd}}$ showing both real space hoppings and the Fock space structure. Solid (green) and dashed (brown) arrows represent right hops with strength J_2 and left hops with strength J_1 , respectively. The numbers in blue show the scaling factors of the states of the states, required for the similarity transformation \mathcal{S} . This gives an example of the second type of connectivity. (b) Connection diagram in Fock space of $\tilde{\mathcal{H}}_f^{\text{odd}}$ after the similarity transformation is carried out. Both the right and left hops, indicated by double-headed blue arrows, have strengths $\sqrt{J^2 - \gamma^2}$ and hence the structure is Hermitian. (c) Same as (a) but now for $\mathcal{H}_{HN,f}^{\text{even}}$ in the (even)(even) sector. It can be seen that (c) is related to (a) by \mathcal{R} . After carrying out the similarity transformation \mathcal{S} , one gets a Hermitian structure like that of (b) for the (even)(even) sector. (d) A closed loop from the $N_d = 1$ sector of the half filled $L = 10$ chain in which the defects retrace back their paths to return to their initial position. This is an example of the first type of connectivity. Panels (a)–(c) correspond to the $N_d = 1$ sector of a half filled $L = 6$ chain.

as $\{|(1)(3)\rangle, |(1)(5)\rangle, |(3)(5)\rangle, |(3)(1)\rangle, |(5)(1)\rangle, |(5)(3)\rangle\}$. It is worthwhile to note that the labeling scheme for the states followed here is the same as that outlined in the main text. In this basis, the Hamiltonian $\mathcal{H}_{HN,f}^{\text{odd}}$ reads as

$$\mathcal{H}_{HN,f}^{\text{odd}} = \begin{pmatrix} V_1 & J_2 & 0 & 0 & 0 & J_2 \\ J_1 & V_1 & J_1 & 0 & 0 & 0 \\ 0 & J_2 & V_1 & J_2 & 0 & 0 \\ 0 & 0 & J_1 & V_1 & J_1 & 0 \\ 0 & 0 & 0 & J_2 & V_1 & J_2 \\ J_1 & 0 & 0 & 0 & J_1 & V_1 \end{pmatrix}, \quad (\text{B1})$$

where $J_1 \equiv J - \gamma$ and $J_2 \equiv J + \gamma$. The connectivity diagram corresponding to $\mathcal{H}_{HN,f}^{\text{odd}}$ is shown in Fig. 7(a). This is, in fact, an example of the second type of connectivity mentioned in the previous section wherein a particle defect moves across the entire chain to return to its original position. This structure is reminiscent of a single-particle hopping problem on a one-dimensional ring in Fock space but with different hopping strengths on alternate links. To map this to our familiar hopping problem, we define a similarity transformation

$$\mathcal{S} = \begin{pmatrix} r & 0 & 0 & 0 & 0 & 0 \\ 0 & 1 & 0 & 0 & 0 & 0 \\ 0 & 0 & r & 0 & 0 & 0 \\ 0 & 0 & 0 & 1 & 0 & 0 \\ 0 & 0 & 0 & 0 & r & 0 \\ 0 & 0 & 0 & 0 & 0 & 1 \end{pmatrix}, \quad (\text{B2})$$

with $r = \sqrt{J_2/J_1}$. The scalings are also shown in Fig. 7(a) in blue. It is straightforward to see that, under this

transformation, $\mathcal{H}_{HN,f}^{\text{odd}}$ assumes a Hermitian structure given by

$$\tilde{\mathcal{H}}_{HN,f}^{\text{odd}} = \mathcal{S}^{-1} \mathcal{H}_{HN,f}^{\text{odd}} \mathcal{S} = \begin{pmatrix} V_1 & \alpha & 0 & 0 & 0 & \alpha \\ \alpha & V_1 & \alpha & 0 & 0 & 0 \\ 0 & \alpha & V_1 & \alpha & 0 & 0 \\ 0 & 0 & \alpha & V_1 & \alpha & 0 \\ 0 & 0 & 0 & \alpha & V_1 & \alpha \\ \alpha & 0 & 0 & 0 & \alpha & V_1 \end{pmatrix}, \quad (\text{B3})$$

where $\alpha = \sqrt{J^2 - \gamma^2}$.

The corresponding connectivity structure in Fock space is shown in Fig. 7(b). This, of course, admits of a real spectrum and the eigenvalues can be readily written down as $\mathcal{E}_k = V_1 + 2\sqrt{J^2 - \gamma^2} \cos(k)$. Here the fictitious lattice spacing is taken to be unity and $k = -\pi + m\pi/3$, with $m = 0, 1, \dots, 5$. The eigenvectors $|k\rangle$ of the original problem can be recovered using the similarity transformation \mathcal{S} .

It is useful to note here that the (even)(even) sector is related to the (odd)(odd) sector through a translation by one lattice spacing \mathcal{R} . This is evident on comparing the connection diagrams in Figs. 7(a) and 7(c). Hence $\mathcal{H}_{HN,f}^{\text{even}}$ has exactly the same structure and spectrum as that of $\mathcal{H}_{HN,f}^{\text{odd}}$. Equivalently, $\mathcal{H}_{HN,f}^{N_d=1} = \mathcal{H}_{HN,f}^{\text{odd}} \oplus \mathcal{H}_{HN,f}^{\text{even}}$ is invariant under \mathcal{R} . This property would be significant in the next section.

Before closing this section, we chalk out examples of the other types of connectivities discussed in the main text. Figure 7(d) illustrates the situation where a particle defect completes a loop by retracing back its path. This gives an

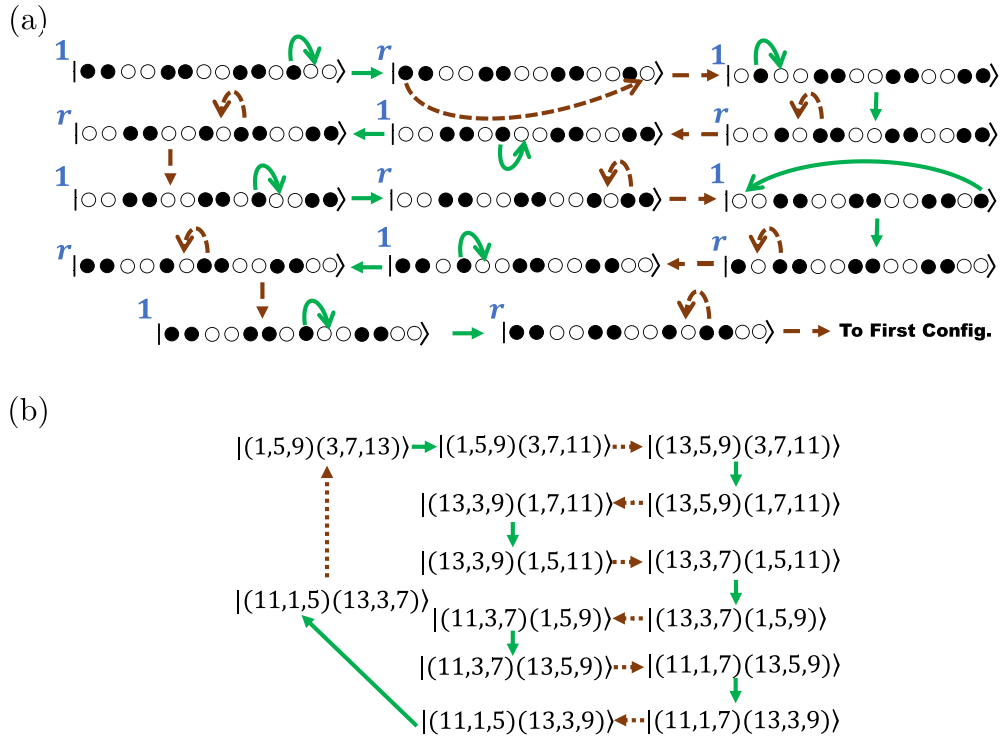


FIG. 8. (a) Closed loop from the $N_d = 3$ sector of the half filled $L = 14$ chain where the defects permute their positions to reach the initial configuration. This is an example of the third kind of connectivity as specified in the main text. Solid (green) and dashed (brown) arrows represent right hops with strength J_2 and left hops with strength J_1 , respectively. The numbers in blue show the scaling factors of the states, required for the similarity transformation. (b) The same connectivity diagram in the Fock space with the states labeled according to the labeling scheme used in the main text.

example of the first type of connectivity discussed in the main text. Figure 8 shows a case where multiple defects exchange their positions in order to complete the loop. This is an example of the third type of connectivity. It is worth noting that, in all these three cases, there are an equal number of right hops and left hops, which makes the similarity transformation possible. As the system size increases, more complicated connection diagrams emerge. However, any closed loop in these connection diagrams will fall in one of these three classes or will be some combination of these three and hence will admit of this general feature.

APPENDIX C: SYMMETRY PROTECTION AND HIDDEN HERMITICITY

We use this section to illustrate with a concrete example the symmetry protection of the real eigenvalues once we move out of the limit of fragmentation of $\mathcal{H}_{HN,f}$ (i.e., infinite V_1) and consider large but finite V_1 effects.

We again consider the $N_d = 1$ sector of the half filled chain of length $L = 6$, whose spectrum was discussed in the previous section. Corresponding to the eigenvalue $\mathcal{E}_{\pi/3}$, there would be four degenerate states of $\mathcal{H}_{HN,f}$, namely $|\psi_{1,2}\rangle_o$ and $|\psi_{1,2}\rangle_e$:

$$|\psi_{1}\rangle_o = \frac{1}{\sqrt{3}}(r\mathcal{C}|(1)(3)\rangle - \mathcal{C}|(1)(5)\rangle - r|(3)(5)\rangle - \mathcal{C}|(3)(1)\rangle + r\mathcal{C}|(5)(1)\rangle + |(5)(3)\rangle),$$

$$|\psi_{2}\rangle_o = \frac{1}{\sqrt{3}}\mathcal{S}(r|(1)(3)\rangle + |(1)(5)\rangle - |(3)(1)\rangle - r|(5)(1)\rangle),$$

$$|\psi_{1}\rangle_e = \frac{1}{\sqrt{3}}(r\mathcal{C}|(2)(4)\rangle - \mathcal{C}|(2)(6)\rangle - r|(4)(6)\rangle - \mathcal{C}|(4)(2)\rangle + r\mathcal{C}|(6)(2)\rangle + |(6)(4)\rangle),$$

$$|\psi_{2}\rangle_e = \frac{1}{\sqrt{3}}\mathcal{S}(r|(2)(4)\rangle + |(2)(6)\rangle - |(4)(2)\rangle - r|(6)(2)\rangle),$$

where $r = (J_2/J_1)^{1/2}$, $\mathcal{C} = \cos \frac{\pi}{3}$, and $\mathcal{S} = \sin \frac{\pi}{3}$.

The first two states are from the (odd)(odd) sector and lie in the subspace spanned by $|k = \pm \frac{\pi}{3}\rangle$, which are related by \mathcal{PC} symmetry. This can be seen easily considering that, under \mathcal{PC} , $\{|(1)(3)\rangle \leftrightarrow |(3)(5)\rangle, |(3)(1)\rangle \leftrightarrow |(5)(3)\rangle, |(1)(5)\rangle \leftrightarrow |(1)(5)\rangle, |(5)(1)\rangle \leftrightarrow |(5)(1)\rangle\}$. The same can be said about the last two states which lie in the (even)(even) sector. States from the (odd)(odd) sector and (even)(even) sector are related by \mathcal{R} , viz. $|\psi_{1(2)}\rangle_e = \mathcal{R}|\psi_{1(2)}\rangle_o$. It is useful to note here that in addition $(\mathcal{PC})^2 = \mathcal{I}$ and $\mathcal{R}^2|\psi_{1(2)}\rangle_{o,e} = |\psi_{1(2)}\rangle_{o,e}$.

We consider the matrix representation of the second order correction, $\mathcal{H}_{HN}^{(2)}$, in this degenerate subspace. Enumerating the basis as $\{|\psi_{1o}\rangle, |\psi_{2o}\rangle, |\psi_{1e}\rangle, |\psi_{2e}\rangle\}$, $\mathcal{H}_{HN}^{(2)}$ reads

$$\mathcal{H}_{HN}^{(2)} = \begin{pmatrix} \mu & 0 & \nu & \lambda \\ 0 & \mu & -\lambda & \nu \\ \nu & -\lambda & \mu & 0 \\ \lambda & \nu & 0 & \mu \end{pmatrix}, \quad (\text{C1})$$

where $\mu = -\frac{J_1 J_2}{V_1}$, $\nu = -\frac{1}{4V_1}(rJ_1^2 + \frac{J_2^2}{r})$, and $\lambda = \frac{\sqrt{3}}{4V_1}(rJ_1^2 + \frac{J_2^2}{r})$. This is Hermitian and admits of real spectrum. This Hermiticity is expected to hold order by order in perturbation since Eq. (4) in the main text is true for exact \mathcal{H}_{HN} . Thus the reality of the spectrum is guaranteed within this subspace.

There remains a second possibility in which these degeneracies might be accidental, i.e., not related by any symmetry, at some point in parameter space. However, we would argue here that such accidental degeneracies are not possible in generic integrable or nonintegrable systems. In case of generic finite-sized nonintegrable systems, one generally expects level repulsion leading to finite gaps in the spectrum, which protects the reality of the eigenspectrum at finite V_1 . These gaps decrease with increasing size as pointed out in the main text; consequently, we expect V_c to diverge in the thermodynamic limit. And in case of an integrable model, a generic crossing between two eigenstates involves eigenstates from different conserved charge sectors. The full Hamiltonian, being integrable, cannot connect between states in different sectors at any order in $1/V_1$. Thus there is no matrix element between them once V_1 is lowered. For our case, we have not observed any occurrence of accidental degeneracy.

APPENDIX D: BOUNDARY CONDITION, SYMMETRY BREAKING, AND COMPLEX EIGENVALUES

So far, we have considered PBC for odd filling and anti-PBC for even filling. In this section, we show that choosing the opposite set of boundary conditions breaks the translational invariance of the full Hamiltonian \mathcal{H}_{HN} and results in complex eigenvalues for any finite value of V_1 . This happens even though $\mathcal{H}_{HN,f}$ has real eigenvalues just as in the case of the standard boundary condition. This is an example where there is no sufficient symmetry protection in the degenerate subspace of $\mathcal{H}_{HN,f}$ and therefore V_c is trivially infinite, because any finite V_1 will lead to complex eigenvalues.

For illustration purposes, we consider a half filled chain of length $L = 4$ with PBC. Choosing the basis as $\{|0\rangle, |\bar{0}\rangle, |(1)(3)\rangle, |(2)(4)\rangle, |(3)(1)\rangle, |(4)(2)\rangle\}$, the Hamiltonian \mathcal{H}_{HN} can be written as

$$\mathcal{H}_{HN} = \begin{pmatrix} 0 & 0 & -J_1 & J_2 & J_1 & J_2 \\ 0 & 0 & J_2 & J_1 & -J_2 & J_1 \\ -J_2 & J_1 & V_1 & 0 & 0 & 0 \\ J_1 & J_2 & 0 & V_1 & 0 & 0 \\ J_2 & -J_1 & 0 & 0 & V_1 & 0 \\ J_1 & J_2 & 0 & 0 & 0 & V_1 \end{pmatrix}, \quad (\text{D1})$$

where $|0\rangle \equiv |\circ \bullet \bullet \bullet\rangle$ and $|\bar{0}\rangle \equiv |\bullet \circ \circ \circ\rangle$. The corresponding connection diagram is shown in Fig. 9(a). It can be readily verified from the matrix structure as well as from the connection diagram that \mathcal{H} is not invariant under \mathcal{R} , which maps $|0\rangle \leftrightarrow |\bar{0}\rangle$ and $|(1)(3)\rangle \rightarrow |(2)(4)\rangle \rightarrow |(3)(1)\rangle \rightarrow |(4)(2)\rangle \rightarrow |(1)(3)\rangle$.

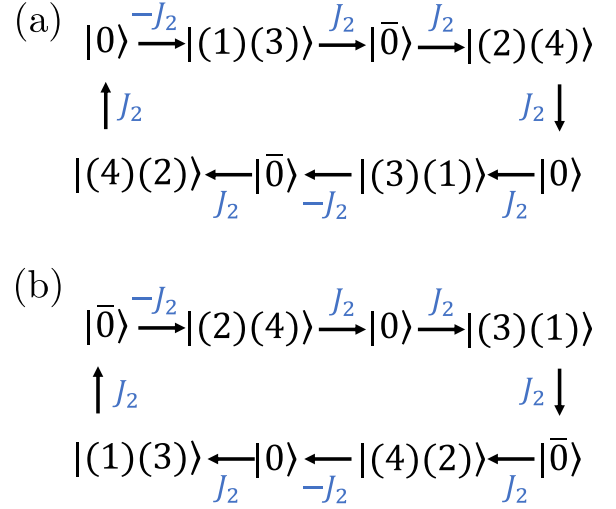


FIG. 9. (a) Fock space connectivity diagram corresponding to the full Hamiltonian \mathcal{H}_{HN} for $L = 4$ with periodic boundary condition. Letters in blue above the arrows show the hopping strength for that particular hop. (b) The fate of the connectivity diagram on application of the one-site lattice translation operator \mathcal{R} . Comparison of the two figures clearly show that \mathcal{H}_{HN} with this boundary condition is not invariant under \mathcal{R} . See text for details.

However, $\mathcal{H}_{HN,f}$ in this basis reads

$$\mathcal{H}_{HN,f} = \begin{pmatrix} 0 & 0 & 0 & 0 & 0 & 0 \\ 0 & 0 & 0 & 0 & 0 & 0 \\ 0 & 0 & V_1 & 0 & 0 & 0 \\ 0 & 0 & 0 & V_1 & 0 & 0 \\ 0 & 0 & 0 & 0 & V_1 & 0 \\ 0 & 0 & 0 & 0 & 0 & V_1 \end{pmatrix}. \quad (\text{D2})$$

This is trivially Hermitian in this case because all the basis states are annihilated by the constrained hopping terms in $\mathcal{H}_{HN,f}$. Such states are termed as frozen states in the field of fragmentation physics. The energy eigenstates can be chosen to be the basis states and they are doubly degenerate in the $N_d = 0$ sector and exhibit fourfold degeneracy in the $N_d = 1$ sector.

We now consider the representation of the second-order correction to \mathcal{H}_{HN} in both these degenerate subspaces:

$$\mathcal{H}_{HN}^{(2)} = \begin{pmatrix} 4\mu & -2\delta & 0 & 0 & 0 & 0 \\ 2\delta & 4\mu & 0 & 0 & 0 & 0 \\ 0 & 0 & -2\mu & -\delta & 2\mu & -\delta \\ 0 & 0 & \delta & -2\mu & -\delta & -2\mu \\ 0 & 0 & 2\mu & \delta & -2\mu & \delta \\ 0 & 0 & \delta & -2\mu & -\delta & -2\mu \end{pmatrix}, \quad (\text{D3})$$

where $\mu = -\frac{J_1 J_2}{V_1}$ and $\delta = \frac{1}{V_1}(J_2^2 - J_1^2)$. This is non-Hermitian, implying that, for any finite value of V_1 , the eigenspectrum will be complex. Explicitly, the eigenvalues of $\mathcal{H}_{HN,f} + \mathcal{H}_{HN}^{(2)}$ are

$$\epsilon = \left(V_1, V_1, -\frac{4}{V_1}(J \pm i\gamma)^2, V_1 + \frac{4}{V_1}(J \pm i\gamma)^2 \right). \quad (\text{D4})$$

This makes it impossible to have a real eigenspectrum for any finite V_1 ; this fact has been numerically found in Ref. [45].

It is important to note here that $\mathcal{H}_{HN,f}$ yields a real spectrum irrespective of the chosen boundary condition. In the case shown, it is trivially real; in other cases, where the connection diagrams are more complicated, a similarity transformation like the above will smoothly go through giving rise

to a real spectrum. The hidden Hermiticity argument becomes invalid because Eq. (4) of the main text fails, owing to the lack of translational symmetry \mathcal{R} of the full Hamiltonian \mathcal{H}_{HN} . This results in the higher-order corrections being manifestly non-Hermitian in the degenerate subspaces, thereby immediately destroying the reality of the spectrum for any finite V_1 .

- [1] For reviews see, e.g., I. Rotter, *J. Phys. A: Math. Theor.* **42**, 153001 (2009); Y. Ashida, Z. Gong, and M. Ueda, *Adv. Phys.* **69**, 249 (2020); I. Rotter and J. P. Bird, *Rep. Prog. Phys.* **78**, 114001 (2015).
- [2] J. González and R. A. Molina, *Phys. Rev. B* **96**, 045437 (2017); V. Kozii and L. Fu, [arXiv:1708.05841](https://arxiv.org/abs/1708.05841); A. A. Zyuzin and A. Y. Zyuzin, *Phys. Rev. B* **97**, 041203(R) (2018); H. Shen and L. Fu, *Phys. Rev. Lett.* **121**, 026403 (2018); R. A. Molina and J. González, *ibid.* **120**, 146601 (2018); T. Yoshida, R. Peters, and N. Kawakami, *Phys. Rev. B* **98**, 035141 (2018); J. Carlström and E. J. Bergholtz, *Phys. Rev. A* **98**, 042114 (2018).
- [3] T. M. Philip, M. R. Hirsbrunner, and M. J. Gilbert, *Phys. Rev. B* **98**, 155430 (2018); Y. Chen and H. Zhai, *ibid.* **98**, 245130 (2018); K. Moors, A. A. Zyuzin, A. Y. Zyuzin, R. P. Tiwari, and T. L. Schmidt, *ibid.* **99**, 041116(R) (2019); R. Okugawa and T. Yokoyama, *ibid.* **99**, 041202(R) (2019); J. C. Budich, J. Carlstrom, F. K. Kunst, and E. J. Bergholtz, *ibid.* **99**, 041406(R) (2019).
- [4] Z. Yang and J. Hu, *Phys. Rev. B* **99**, 081102(R) (2019); T. Yoshida, R. Peters, N. Kawakami, and Y. Hatsugai, *ibid.* **99**, 121101(R) (2019); Y. Wu, W. Liu, J. Geng, X. Song, X. Ye, C.-K. Duan, X. Rong, and J. Du, *Science* **364**, 878 (2019); P. San-Jose, J. Cayao, E. Prada, and R. Aguado, *Sci. Rep.* **6**, 21427 (2016); Q.-B. Zeng, B. Zhu, S. Chen, L. You, and R. Lu, *Phys. Rev. A* **94**, 022119 (2016); C. Li, X. Z. Zhang, G. Zhang, and Z. Song, *Phys. Rev. B* **97**, 115436 (2018); J. Cayao and A. M. Black-Schaffer, *ibid.* **105**, 094502 (2022); R. Arouca, J. Cayao, and A. M. Black-Schaffer, *ibid.* **108**, L060506 (2023).
- [5] K. Kawabata, Y. Ashida, H. Katsura, and M. Ueda, *Phys. Rev. B* **98**, 085116 (2018); A. Guo, G. J. Salamo, D. Duchesne, R. Morandotti, M. Volatier-Ravat, V. Aimez, G. A. Siviloglou, and D. N. Christodoulides, *Phys. Rev. Lett.* **103**, 093902 (2009); C. E. Rüter, K. G. Makris, R. El-Ganainy, D. N. Christodoulides, M. Segev, and D. Kip, *Nat. Phys.* **6**, 192 (2010); L. Feng, M. Ayache, J. Huang, Y.-L. Xu, M.-H. Lu, Y.-F. Chen, Y. Fainman, and A. Scherer, *Science* **333**, 729 (2011); A. Regensburger, C. Bersch, M.-A. Miri, G. Onishchukov, D. N. Christodoulides, and U. Peschel, *Nature (London)* **488**, 167 (2012).
- [6] L. Feng, Y.-L. Xu, W. S. Fegadolli, M.-H. Lu, J. E. Oliveira, V. R. Almeida, Y.-F. Chen, and A. Scherer, *Nat. Mater.* **12**, 108 (2013); C. Poli, M. Bellec, U. Kuhl, F. Mortessagne, and H. Schomerus, *Nat. Commun.* **6**, 6710 (2015); B. Zhen, C. W. Hsu, Y. Igarashi, L. Lu, I. Kaminer, A. Pick, S.-L. Chua, J. D. Joannopoulos, and M. Soljačić, *Nature (London)* **525**, 354 (2015); H. Zhao, S. Longhi, and L. Feng, *Sci. Rep.* **5**, 17022 (2015); K. Ding, Z. Q. Zhang, and C. T. Chan, *Phys. Rev. B* **92**, 235310 (2015).
- [7] S. Weimann, M. Kremer, Y. Plotnik, Y. Lumer, S. Nolte, K. Makris, M. Segev, M. Rechtsman, and A. Szameit, *Nat. Mater.* **16**, 433 (2017); H. Hodaei, A. U. Hassan, S. Wittek, H. Garcia-Gracia, R. El-Ganainy, D. N. Christodoulides, and M. Khajavikhan, *Nature (London)* **548**, 187 (2017); W. Chen, K. Ozdemir, G. Zhao, J. Wiersig, and L. Yang, *ibid.* **548**, 192 (2017); P. St-Jean, V. Goblot, E. Galopin, A. Lemaître, T. Ozawa, L. Le Gratiet, I. Sagnes, J. Bloch, and A. Amo, *Nat. Photon.* **11**, 651 (2017).
- [8] B. Bahari, A. Ndao, F. Vallini, A. E. Amili, Y. Fainman, and B. K. Le, *Science* **358**, 636 (2017); J. Wang, H. Y. Dong, Q. Y. Shi, W. Wang, and K. H. Fung, *Phys. Rev. B* **97**, 014428 (2018); H. Zhou, C. Peng, Y. Yoon, C. W. Hsu, K. A. Nelson, L. Fu, J. D. Joannopoulos, M. Soljačić, and B. Zhen, *Science* **359**, 1009 (2018); M. Parto, S. Wittek, H. Hodaei, G. Harari, M. A. Bandres, J. Ren, M. C. Rechtsman, M. Segev, D. N. Christodoulides, and M. Khajavikhan, *Phys. Rev. Lett.* **120**, 113901 (2018); H. Zhao, P. Miao, M. H. Teimourpour, S. Malzard, R. El-Ganainy, H. Schomerus, and L. Feng, *Nat. Commun.* **9**, 981 (2018).
- [9] G. Harari, M. A. Bandres, Y. Lumer, M. C. Rechtsman, Y. D. Chong, M. Khajavikhan, D. N. Christodoulides, and M. Segev, *Science* **359**, eaar4003 (2018); M. A. Bandres, S. Wittek, G. Harari, M. Parto, J. Ren, M. Segev, D. N. Christodoulides, and M. Khajavikhan, *ibid.* **359**, eaar4005 (2018); M. Pan, H. Zhao, P. Miao, S. Longhi, and L. Feng, *Nat. Commun.* **9**, 1308 (2018); L. Jin and Z. Song, *Phys. Rev. Lett.* **121**, 073901 (2018); S. Malzard and H. Schomerus, *Phys. Rev. A* **98**, 033807 (2018); Z. Oztas and C. Yuce, *ibid.* **98**, 042104 (2018).
- [10] M. Kremer, T. Biesenthal, L. J. Maczewsky, M. Heinrich, R. Thomale, and A. Szameit, *Nat. Commun.* **10**, 435 (2019); K. Y. Bliokh, D. Leykam, M. Lein, and F. Nori, *ibid.* **10**, 580 (2019); S. Wang, B. Hou, W. Lu, Y. Chen, Z. Zhang, and C. Chan, *ibid.* **10**, 832 (2019); S. Chen, W. Zhang, B. Yang, T. Wu, and X. Zhang, *Sci. Rep.* **9**, 5551 (2019); T. E. Lee and C.-K. Chan, *Phys. Rev. X* **4**, 041001 (2014); Y. Xu, S.-T. Wang, and L.-M. Duan, *Phys. Rev. Lett.* **118**, 045701 (2017); Y. Ashida, S. Furukawa, and M. Ueda, *Nat. Commun.* **8**, 15791 (2017); Z. Gong, Y. Ashida, K. Kawabata, K. Takasan, S. Higashikawa, and M. Ueda, *Phys. Rev. X* **8**, 031079 (2018); M. Nakagawa, N. Kawakami, and M. Ueda, *Phys. Rev. Lett.* **121**, 203001 (2018); K. Takata and M. Notomi, *ibid.* **121**, 213902 (2018); L. Pan, S. Chen, and X. Cui, *Phys. Rev. A* **99**, 011601(R) (2019).
- [11] J. Li, A. K. Harter, J. Liu, L. de Melo, Y. N. Joglekar, and L. Luo, *Nat. Commun.* **10**, 855 (2019); T. Liu, Y.-R. Zhang, Q. Ai, Z. Gong, K. Kawabata, M. Ueda, and F. Nori, *Phys. Rev. Lett.* **122**, 076801 (2019); M. S. Rudner and L. S. Levitov, *ibid.* **102**, 065703 (2009); J. M. Zeuner, M. C. Rechtsman, Y. Plotnik, Y. Lumer, S. Nolte, M. S. Rudner, M. Segev, and A. Szameit, *ibid.* **115**, 040402 (2015); K. Mochizuki, D. Kim, and H. Obuse, *Phys. Rev. A* **93**, 062116 (2016); L. Xiao, X. Zhan, Z. Bian, K.

- Wang, X. Zhang, X. Wang, J. Li, K. Mochizuki, D. Kim, N. Kawakami *et al.*, *Nat. Phys.* **13**, 1117 (2017).
- [12] N. Hatano and D. R. Nelson, *Phys. Rev. Lett.* **77**, 570 (1996); *Phys. Rev. B* **56**, 8651 (1997); **58**, 8384 (1998).
- [13] J. A. S. Lourenço, R. L. Eneias, and R. G. Pereira, *Phys. Rev. B* **98**, 085126 (2018); E. I. Rosenthal, N. K. Ehrlich, M. S. Rudner, A. P. Higginbotham, and K. W. Lehnert, *ibid.* **97**, 220301(R) (2018); M. Wang, L. Ye, J. Christensen, and Z. Liu, *Phys. Rev. Lett.* **120**, 246601 (2018).
- [14] M. Ezawa, *Phys. Rev. B* **99**, 121411(R) (2019); **99**, 201411(R) (2019); **100**, 045407 (2019).
- [15] L. Zhou, Q. H. Wang, H. Wang, and J. Gong, *Phys. Rev. A* **98**, 022129 (2018); L. Zhou and Q. Du, *New J. Phys.* **23**, 063041 (2021); B. Zhu, Y. Ke, H. Zhong, and C. Lee, *Phys. Rev. Res.* **2**, 023043 (2020); L. Zhou and J. Gong, *Phys. Rev. B* **98**, 205417 (2018); L. Zhou, *ibid.* **100**, 184314 (2019); L. Zhou, Y. Gu, and J. Gong, *ibid.* **103**, L041404 (2021).
- [16] L. Zhou and W. Han, *Phys. Rev. B* **106**, 054307 (2022); C-H Liu, C.-H. Liu, and S. Chen, *ibid.* **105**, 214305 (2022); L. Zhou, R. W. Bomantara, and S. Wu, *SciPost Phys.* **13**, 015 (2022).
- [17] S. Zamani, R. Jafari, and A. Langari, *Phys. Rev. B* **102**, 144306 (2020); R. Jafari and A. Akbari, *Phys. Rev. A* **103**, 012204 (2021); K. Yang, L. Zhou, W. Ma, X. Kong, P. Wang, X. Qin, X. Rong, Y. Wang, F. Shi, J. Gong, and J. Du, *Phys. Rev. B* **100**, 085308 (2019); D. Chowdhury, A. Banerjee, and A. Narayan, *Phys. Rev. A* **103**, L051101 (2021).
- [18] P. He and Z.-H. Huang, *Phys. Rev. A* **102**, 062201 (2020); S. Longhi, *J. Phys. A: Math. Theor.* **50**, 505201 (2017).
- [19] X. Turkeshi and M. Schiro, *Phys. Rev. B* **107**, L020403 (2023); T. Banerjee and K. Sengupta, *ibid.* **107**, 155117 (2023).
- [20] J. Ren, P. Hanggi, and B. Li, *Phys. Rev. Lett.* **104**, 170601 (2010); J. Ren, S. Liu, and B. Li, *ibid.* **108**, 210603 (2012); H. Xu, D. Mason, L. Jiang, and J. G. E. Harris, *Nature (London)* **537**, 80 (2016); Z. Wang, J. Chen, and J. Ren, *Phys. Rev. E* **106**, L032102 (2022); L. J. Fernández-Alcazar, R. Kononchuk, H. Li, and T. Kottos, *Phys. Rev. Lett.* **126**, 204101 (2021).
- [21] For reviews see, e.g., E. J. Bergholtz, J. C. Budich, and F. K. Kunst, *Rev. Mod. Phys.* **93**, 015005 (2021); W. D. Heiss, *J. Phys. A: Math. Theor.* **45**, 444016 (2012); M. Müller and I. Rotter, *ibid.* **41**, 244018 (2008).
- [22] Y. C. Hu and T. L. Hughes, *Phys. Rev. B* **84**, 153101 (2011); K. Esaki, M. Sato, K. Hasebe, and M. Kohmoto, *ibid.* **84**, 205128 (2011); T. E. Lee, *Phys. Rev. Lett.* **116**, 133903 (2016); D. Leykam, K. Y. Bliokh, C. Huang, Y. D. Chong, and F. Nori, *ibid.* **118**, 040401 (2017); V. M. Martínez Alvarez, J. E. Barrios Vargas, and L. E. F. Foa Torres, *Phys. Rev. B* **97**, 121401(R) (2018); Y. Xiong, *J. Phys. Commun.* **2**, 035043 (2018); H. Shen, B. Zhen, and L. Fu, *Phys. Rev. Lett.* **120**, 146402 (2018).
- [23] C. Yuce, *Phys. Rev. A* **97**, 042118 (2018); C. Yin, H. Jiang, L. Li, R. Lu, and S. Chen, *ibid.* **97**, 052115 (2018); C. Yuce, *ibid.* **98**, 012111 (2018); F. K. Kunst, E. Edvardsson, J. C. Budich, and E. J. Bergholtz, *Phys. Rev. Lett.* **121**, 026808 (2018); S. Yao, F. Song, and Z. Wang, *ibid.* **121**, 136802 (2018); K. Kawabata, K. Shiozaki, and M. Ueda, *Phys. Rev. B* **98**, 165148 (2018); C. Yuce and Z. Oztas, *Sci. Rep.* **8**, 17416 (2018).
- [24] S. Yao and Z. Wang, *Phys. Rev. Lett.* **121**, 086803 (2018).
- [25] K. Kawabata, S. Higashikawa, Z. Gong, Y. Ashida, and M. Ueda, *Nat. Commun.* **10**, 297 (2019); L. Jin and Z. Song, *Phys. Rev. B* **99**, 081103(R) (2019); H. Wang, J. Ruan, and H. Zhang, *ibid.* **99**, 075130 (2019); D. S. Borgnia, A. J. Kruchkov, and R.-J. Slager, *Phys. Rev. Lett.* **124**, 056802 (2020); Z. Ozcakmakli Turker and C. Yuce, *Phys. Rev. A* **99**, 022127 (2019); E. Edvardsson, F. K. Kunst, and E. J. Bergholtz, *Phys. Rev. B* **99**, 081302(R) (2019).
- [26] C.-H. Liu, H. Jiang, and S. Chen, *Phys. Rev. B* **99**, 125103 (2019); C. H. Lee and R. Thomale, *ibid.* **99**, 201103(R) (2019); F. K. Kunst and V. Dwivedi, *ibid.* **99**, 245116 (2019); K. Yokomizo and S. Murakami, *Phys. Rev. Lett.* **123**, 066404 (2019).
- [27] R. Nehra and D. Roy, *Phys. Rev. B* **105**, 195407 (2022); K. Kawabata, K. Shiozaki, and S. Ryu, *ibid.* **105**, 165137 (2022); B. Li, S.-X. Chen, and A.-L. Li, *ApJ* **928**, 33 (2022).
- [28] A. Mostafazadeh, *J. Math. Phys.* **43**, 205 (2002).
- [29] A. Mostafazadeh, *J. Math. Phys.* **43**, 2814 (2002).
- [30] C. M. Bender, *Rep. Prog. Phys.* **70**, 947 (2007).
- [31] A. A. Zyablovsky, A. P. Vinogradov, A. A. Pukhov, A. V. Dorofeenko, and A. A. Lisyansky, *Phys. Usp.* **57**, 1063 (2014).
- [32] S. K. Özdemir, S. Rotter, F. Nori, and L. Yang, *Nat. Mater.* **18**, 783 (2019).
- [33] V. Khemani, M. Hermele, and R. Nandkishore, *Phys. Rev. B* **101**, 174204 (2020).
- [34] P. Sala, T. Rakovszky, R. Verresen, M. Knap, and F. Pollmann, *Phys. Rev. X* **10**, 011047 (2020).
- [35] T. Rakovszky, P. Sala, R. Verresen, M. Knap, and F. Pollmann, *Phys. Rev. B* **101**, 125126 (2020).
- [36] Z.-C. Yang, F. Liu, A. V. Gorshkov, and T. Iadecola, *Phys. Rev. Lett.* **124**, 207602 (2020).
- [37] G. De Tomasi, D. Hetterich, P. Sala, and F. Pollmann, *Phys. Rev. B* **100**, 214313 (2019).
- [38] P. Frey, L. Hackl, and S. Rachel, *Phys. Rev. B* **106**, L220301 (2022).
- [39] S. Moudgalya and O. I. Motrunich, *Phys. Rev. X* **12**, 011050 (2022); D. T. Stephen, O. Hart, and R. M. Nandkishore, *arXiv:2209.03966*; D. Hahn, P. A. McClarty, and D. J. Luitz, *SciPost Phys.* **11**, 074 (2021); N. Regnault and B. A. Bernevig, *arXiv:2210.08019*; D. D. Vu, K. Huang, X. Li, and S. Das Sarma, *Phys. Rev. Lett.* **128**, 146601 (2022).
- [40] T. Kohlert, S. Scherg, P. Sala, F. Pollmann, B. H. Madhusudhana, I. Bloch, and M. Aidelsburger, *Phys. Rev. Lett.* **130**, 010201 (2023).
- [41] B. Mukherjee, D. Banerjee, K. Sengupta, and A. Sen, *Phys. Rev. B* **104**, 155117 (2021); R. Wang and D. Klabjan, *arXiv:2210.05607*.
- [42] J. Lehmann, P. Sala, F. Pollmann, and T. Rakovszky, *SciPost Phys.* **14**, 140 (2023).
- [43] A. Chattopadhyay, B. Mukherjee, K. Sengupta, and A. Sen, *SciPost Phys.* **14**, 146 (2023).
- [44] S. Ghosh, I. Paul, and K. Sengupta, *Phys. Rev. Lett.* **130**, 120401 (2023).
- [45] S.-B. Zhang, M. M. Denner, T. Bzdušek, M. A. Sentef, and T. Neupert, *Phys. Rev. B* **106**, L121102 (2022).
- [46] R. G. Dias, *Phys. Rev. B* **62**, 7791 (2000).
- [47] M. Rigol, V. Dunjko, and M. Olshanii, *Nature (London)* **452**, 854 (2008).
- [48] E. Khatami, G. Pupillo, M. Srednicki, and M. Rigol, *Phys. Rev. Lett.* **111**, 050403 (2013).